DEVELOPMENT AND DISEASE

An *Fgf8* mouse mutant phenocopies human 22q11 deletion syndrome

Deborah U. Frank[1], Lori K. Fotheringham[1], Judson A. Brewer[2], Louis J. Muglia[2], Martin Tristani-Firouzi[1], Mario R. Capecchi[3] and Anne M. Moon[1,4,*]

[1]Department of Pediatrics, University of Utah School of Medicine, Salt Lake City, UT 84112, USA
[2]Departments of Pediatrics, Molecular Biology and Pharmacology, Washington University School of Medicine, St Louis, MO, USA
[3]Howard Hughes Medical Institute and Department of Human Genetics, University of Utah School of Medicine, Salt Lake City, UT 84112, USA
[4]Program in Human Molecular Biology and Genetics, University of Utah School of Medicine, Salt Lake City, UT 84112, USA
*Author for correspondence (e-mail: anne.moon@genetics.utah.edu)

SUMMARY

Deletion of chromosome 22q11, the most common microdeletion detected in humans, is associated with a life-threatening array of birth defects. Although 90% of affected individuals share the same three megabase deletion, their phenotype is highly variable and includes craniofacial and cardiovascular anomalies, hypoplasia or aplasia of the thymus with associated deficiency of T cells, hypocalcemia with hypoplasia or aplasia of the parathyroids, and a variety of central nervous system abnormalities. Because ablation of neural crest in chicks produces many features of the deletion 22q11 syndrome, it has been proposed that haploinsufficiency in this region impacts neural crest function during cardiac and pharyngeal arch development. Few factors required for migration, survival, proliferation and subsequent differentiation of pharyngeal arch neural crest and mesoderm-derived mesenchyme into their respective cardiovascular, musculoskeletal, and glandular derivatives have been identified. However, the importance of epithelial-mesenchymal interactions and pharyngeal endoderm function is becoming increasingly clear.

Fibroblast growth factor 8 is a signaling molecule expressed in the ectoderm and endoderm of the developing pharyngeal arches and known to play an important role in survival and patterning of first arch tissues. We demonstrate a dosage-sensitive requirement for FGF8 during development of pharyngeal arch, pharyngeal pouch and neural crest-derived tissues. We show that FGF8 deficient embryos have lethal malformations of the cardiac outflow tract, great vessels and heart due, at least in part, to failure to form the fourth pharyngeal arch arteries, altered expression of *Fgf10* in the pharyngeal mesenchyme, and abnormal apoptosis in pharyngeal and cardiac neural crest.

The *Fgf8* mutants described herein display the complete array of cardiovascular, glandular and craniofacial phenotypes seen in human deletion 22q11 syndromes. This represents the first single gene disruption outside the typically deleted region of human chromosome 22 to fully recapitulate the deletion 22q11 phenotype. FGF8 may operate directly in molecular pathways affected by deletions in 22q11 or function in parallel pathways required for normal development of pharyngeal arch and neural crest-derived tissues. In either case, *Fgf8* may function as a modifier of the 22q11 deletion and contribute to the phenotypic variability of this syndrome.

Key words: 22q11 deletion syndromes, Pharyngeal arches, FGF8, Pharyngeal arch artery, Congenital heart disease, Truncus arteriosus, Interrupted aortic arch, Outflow tract, Endoderm, Immunodeficiency

INTRODUCTION

Pharyngeal arches are transient bulges of tissue in the neck of vertebrate embryos consisting of mesenchyme separated by membranous clefts in which the surface ectoderm directly apposes evaginations of the pharyngeal endoderm (the pharyngeal pouches). Pharyngeal arch mesenchyme is derived from neural crest cells and paraxial mesoderm. Neural crest-derived mesenchyme gives rise to the skeletal structures and to pericytes and smooth muscle cells of the arch arteries (Birgbauer et al., 1995; Etchevers et al., 1999). Some neural

crest mesenchyme populates the arches only transiently, en route to final destinations in the outflow tract and heart (Epstein et al., 2000; Jiang et al., 2000). The mesoderm-derived mesenchyme contributes muscular and endothelial precursors to each arch. A vessel forms within each arch and circulates blood from the heart to the bilateral dorsal aortae. This pharyngeal arch arterial system is a transient, initially symmetrical array of vessels; the most rostral vessels in the first and second arches largely regress while the caudal pharyngeal arch arteries (PAAs) are extensively remodeled into adult vascular structures, including the subclavian arteries and

the arch of the aorta. Aberrant formation and/or remodeling of the pharyngeal arch arterial system results in congenital vascular malformations ranging in severity from clinically insignificant to lethal.

A growing body of evidence indicates that signals from pharyngeal endoderm pattern the arch neural crest and mesoderm (Couly et al., 2002; LeDouarin, 1982; Piotrowski and Nusslein-Volhard, 2000; Thomas et al., 1998; Veitch et al., 1999; Wendling et al., 2000). This tissue expresses signaling molecules such as bone morphogenetic proteins, fibroblast growth factors (FGFs), Sonic hedgehog, and transcription factors including *Hox A3*, *Pax1*, *Pax9* and *Tbx1* (Dietrich and Gruss, 1995; Garg et al., 2001; Manley and Capecchi, 1998; Peters et al., 1998). Pharyngeal pouch endoderm gives rise to the thyroid, parathyroid and thymus glands. Interactions between neural crest and endoderm are important for early thymic and parathyroid development (Bockman and Kirby, 1984; Le Douarin and Jotereau, 1975; LeLievre and LeDouarin, 1975) and later proliferation of the thymic epithelium has been shown to be dependent on FGF signaling (Revest et al., 2001).

Haploinsufficiency of chromosome 22q11(del22q11) is the genetic abnormality shared by the majority of individuals diagnosed with DiGeorge sequence (DiGeorge, 1965), Velocardiofacial syndrome (Shprintzen et al., 1978) and Conotruncal anomaly face syndrome (Burn et al., 1993) (for reviews, see Emanuel et al., 2001; Lindsay, 2001; Scambler, 2000). The craniofacial, cardiovascular and glandular phenotypes that characterize these individuals indicate that all pharyngeal arch-derived structures may be affected. Affected individuals often present in the neonatal period with life-threatening cardiac malformations. Conotruncal defects such as persistent truncus arteriosus and Tetralogy of Fallot are common, as are aortic arch defects including interrupted aortic arch, right aortic arch and vascular ring (Emanuel et al., 2001).

Molecular defects resulting from deletion of genes in del22q11 are hypothesized to adversely affect neural crest function during cardiac and pharyngeal arch development (Emanuel et al., 2001; Robinson, 1975; Van Mierop and Kutsche, 1986). Mechanical ablation of premigratory 'cardiac' neural crest from the posterior hindbrain of chick embryos produces many features of del22q11, including interrupted aortic arch type B and truncus arteriosus (Bockman et al., 1989; Kirby and Waldo, 1990). The results of *Wnt1* and *Pax3* neural crest lineage analyses provide evidence for the existence of a cardiac neural crest population in mammals as well (Epstein et al., 2000; Jiang et al., 2000). Furthermore, mice homozygous for mutations in the neural crest-expressed *Pax3* gene [the *splotch* (Sp^{2h}) mouse] show decreased numbers of migrating cardiac neural crest cells (Conway et al., 1997a; Epstein et al., 2000) and a severe phenotype that includes cardiovascular features of del22q11 (Conway et al., 1997b; Franz, 1989; Goulding et al., 1993).

An enormous effort has been directed towards understanding how haploinsufficiency for the three megabase typically deleted region (TDR, the deletion found in 90% of affected individuals) of chromosome 22 results in the clinically heterogeneous del22q11syndromes. Investigators have attempted to model these syndromes in mice by deleting the region of murine chromosome 16 corresponding to the

TDR (Kimber et al., 1999; Lindsay et al., 1999; Puech et al., 2000). Others inactivated murine orthologs of genes within the TDR (Guris et al., 2001; Jerome and Papaioannou, 2001; Lindsay et al., 2001; Merscher et al., 2001; Saint-Jore et al., 1998). In all cases, heterozygotes were either phenotypically normal or had partial phenotypes with cardiovascular defects that were infrequent and mild, relative to those seen in humans. Twenty five percent of heterozygous mice bearing an engineered deletion on chromosome 16 called *Df1* had vascular malformations, predominantly affecting the right subclavian artery (Lindsay et al., 1999). *Crko1* heterozygotes (homologous to the CRKL locus in the human TDR) were normal, but homozygotes had vascular, thymic, parathyroid and craniofacial malformations (Guris et al., 2001). *Tbx1*, another gene within the TDR, encodes a transcription factor in the T-box family expressed in the endoderm and mesoderm of the pharyngeal arches (Garg et al., 2001). *Tbx1*-null homozygotes display the most severe features of del22q11; 100% of *Tbx1*-null homozygotes had truncus arteriosus and lacked thymus and parathyroid glands (Jerome and Papaioannou, 2001).

Data from murine models and from humans suggest that multiple loci on chromosome 22 or elsewhere may function in the pathogenesis or act as modifiers of the del22q11 phenotype (Yamagishi et al., 1999; Emanuel et al., 2001; Lindsay, 2001; Scambler, 2000). Sequence and microdeletion analysis of nondeleted syndromic individuals has not revealed causal mutations in *Tbx1* or other genes on 22q11 (Chieffo et al., 1997; Wadey et al., 1999; Emanuel et al., 2001). Humans bearing identical deletions have highly variable phenotypes, both with regard to affected structures and presence and severity of cardiovascular disease. Indistinguishable phenotypes have been observed in association with deletions and translocations on chromosome 10p (Gottlieb et al., 1998; Herve et al., 1984) and as the result of teratogenic exposure. Dysfunction of genes that operate in common developmental or genetic pathways may independently generate or modify the 'del22q11 phenotype'.

FGF8 is a secreted signaling molecule expressed in the developing brain, face and limbs, and in the endoderm and ectoderm of the pharyngeal pouches and grooves (Crossley and Martin, 1995; MacArthur et al., 1995). During embryogenesis, epithelially produced FGF8 provides survival, mitogenic, antidifferentiation and patterning signals to adjacent mesenchyme (Moon and Capecchi, 2000; Lewandoski et al., 2000; Trumpp et al., 1999). Ectodermal FGF8 signaling has been demonstrated to regulate mesenchymal gene expression in the first pharyngeal arch (Tucker et al., 1999a; Tucker et al., 1999b); conditional ablation of FGF8 in first arch ectoderm results in craniofacial defects caused by death of first arch neural crest mesenchyme and perturbed expression of patterning genes (Trumpp et al., 1999). Severe hypomorphism for FGF8 results in gastrulation and left-right asymmetry defects (Meyers et al., 1998; Meyers and Martin, 1999). We employ a hypomorphic allele of *Fgf8* to demonstrate that FGF8 performs unique and required roles in development of murine pharyngeal arch and pouch-derived structures including the pharyngeal arch arteries (PAAs), cardiac outflow tract, heart, thymus and parathyroids. The constellation of anomalies displayed by these *Fgf8* hypomorphic mutants is a remarkably complete phenocopy of human del22q11 syndrome. These

animals provide an excellent model system in which to examine molecular and cellular pathways that result in this common and frequently lethal human syndrome.

MATERIALS AND METHODS

Mutant mouse strains

Creation of the hypomorphic and null alleles of *Fgf8* has previously been described (Moon and Capecchi, 2000). The official names for the *Fgf8* null allele (*Fgf8−*) is Fgf8*tm1Mrc* and the for the *Fgf8* hypomorphic allele (*Fgf8*H) is Fgf8*tm2Mrc*. The alleles were created in an SV129 background and were backcrossed 6 or more generations intoC57Bl6. The Wnt1Cre mice (Jiang et al., 2000) were kindly provided by A. McMahon.

Reverse-transcription, PCR amplification

Total RNA was isolated from E10.0 embryos with Trizol reagent (Gibco BRL) according to manufacturer's instructions. One microgram of total RNA was reverse-transcribed with a first-strand cDNA synthesis kit (Omniscript, Qiagen) and 2 µl of the product was amplified with primers 5′-AAGCTCATTGTGGAGACCGAT-3′ and 5′-AGCTCCCGCTGGATTCCTC-3′ for X=28 and X+1=29 cycles to detect F*gf8* cDNA, or with primers 5′CCAGTATGACTCCACTCAC-GGCA 3′ and 5′ATACTTGGCAGGTTTCGCCAGGCG 3′ for X=13 and X+1=14 cycles to detect the GAPDH control cDNA. To assure that the results were quantitative, the cycle number for each primer set was optimized for amplification within the linear range.

Corrosion casting of vasculature

Pregnant females were anesthetized with a lethal dose of Avertin by

intraperitoneal injection and the embryos removed. Thoracotomy was performed and the pericardium opened. Blue Mercox resin and catalyst (Ladd Research Industries #21246 and Benzoyl Peroxide CAS [94-36-0]) were injected into the left ventricle using a pulled glass needle. After allowing the resin to cure for 24 hours, the preparations were placed in Batson's #17 Maceration solution (Polysciences, Warrington, PA; catalog number, 07359) for 48-72 hours until tissues were completely dissolved. The casts were rinsed repeatedly in distilled water and stored in water.
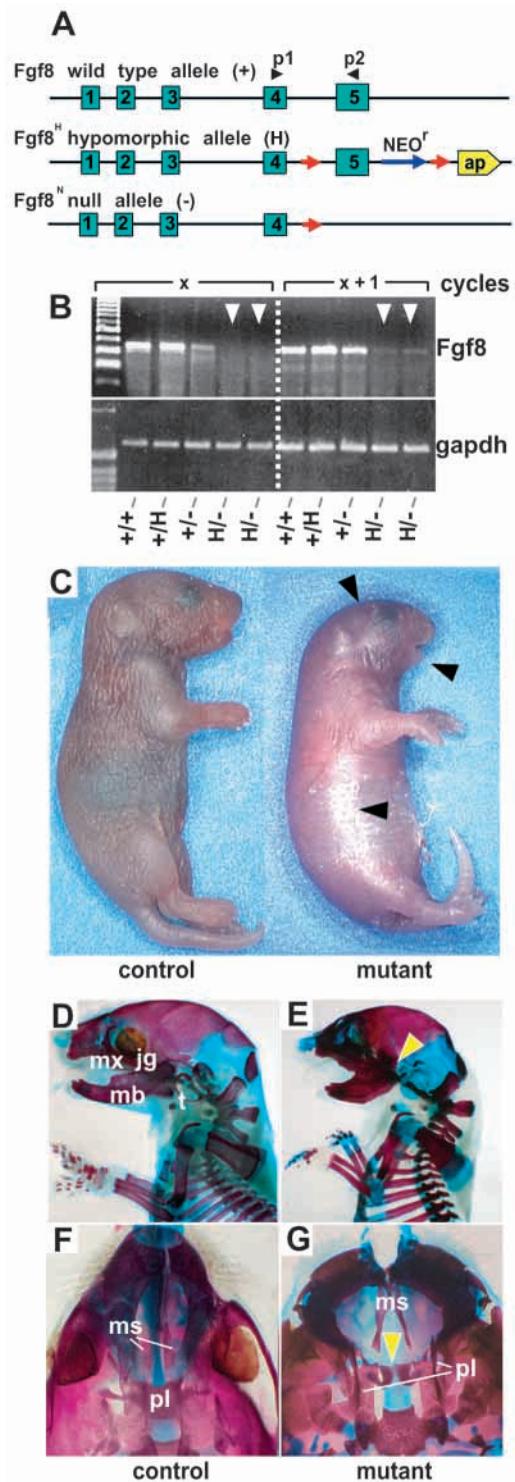

Fig. 1. The presence of the neo^r gene in the 3′untranslated region (UTR) of the *Fgf8* gene has transcriptional and morphological consequences. (A) The *Fgf8*H hypomorphic and *Fgf8−* alleles. The neomycin phosphotransferase gene (neo^r, blue arrow) and alkaline phosphatase reporter gene (AP, yellow block arrowhead) are located in the 3′UTR of *Fgf8*. PCR primers used to amplify exon 5 containing reverse transcription (RT) products are shown as black arrowheads (P1 and P2). LoxP sites are shown as red arrowheads. The null allele lacks *Fgf8* exon 5 as previously described (Moon and Capecchi, 2000). If recombined by Cre recombinase, the *Fgf8*H allele produces the AP reporter regulated by the *Fgf8* promoter. (B) Semi-quantitative RT/PCR of cDNAs prepared by reverse transcription of mRNA isolated from E9.5 embryos. The amount of exon 5 containing *Fgf8* mRNA is decreased in *Fgf8* mutants (*Fgf8*H/−, white arrowheads) when compared with wild type (*Fgf8*+/+), null heterozygote (*Fgf8*+/−) or hypomorph allele heterozygote (*Fgf8*H/+) littermate controls. The results displayed show the amplification products obtained with amplification cycles of X or X+1 to assure that the amplification was performed within the linear range for each product and that the signal obtained was not saturated. The control panel shows RT-PCR products using GAPDH primers and confirms that specimens from the *Fgf8*H/− mutant embryos contain comparable amounts of total mRNA with controls, although the amount of *Fgf8* mRNA in *Fgf8*H/− compound heterozygous, hypomorphic mutants is markedly decreased. (C) Newborn *Fgf8*H/− mutant and *Fgf8*H/+ control. The mutant is smaller, cyanotic and edematous with obvious craniofacial abnormalities (arrowheads). All of the mutants had CNS and mandibular malformations, 30% had a cleft palate.
(D-G) Skeleton preps of *Fgf8*H/− mutant and control. (E) The mutant exhibits micrognathia, fusion of the maxilla (mx), jugal bone (jg) and mandible (mb), and absence of the tympanic ring (t, yellow arrowhead). (G) Cleft palate (arrowhead) in a mutant resulting from failure of fusion of the palatine shelves (pl) with the maxillary shelves (ms).
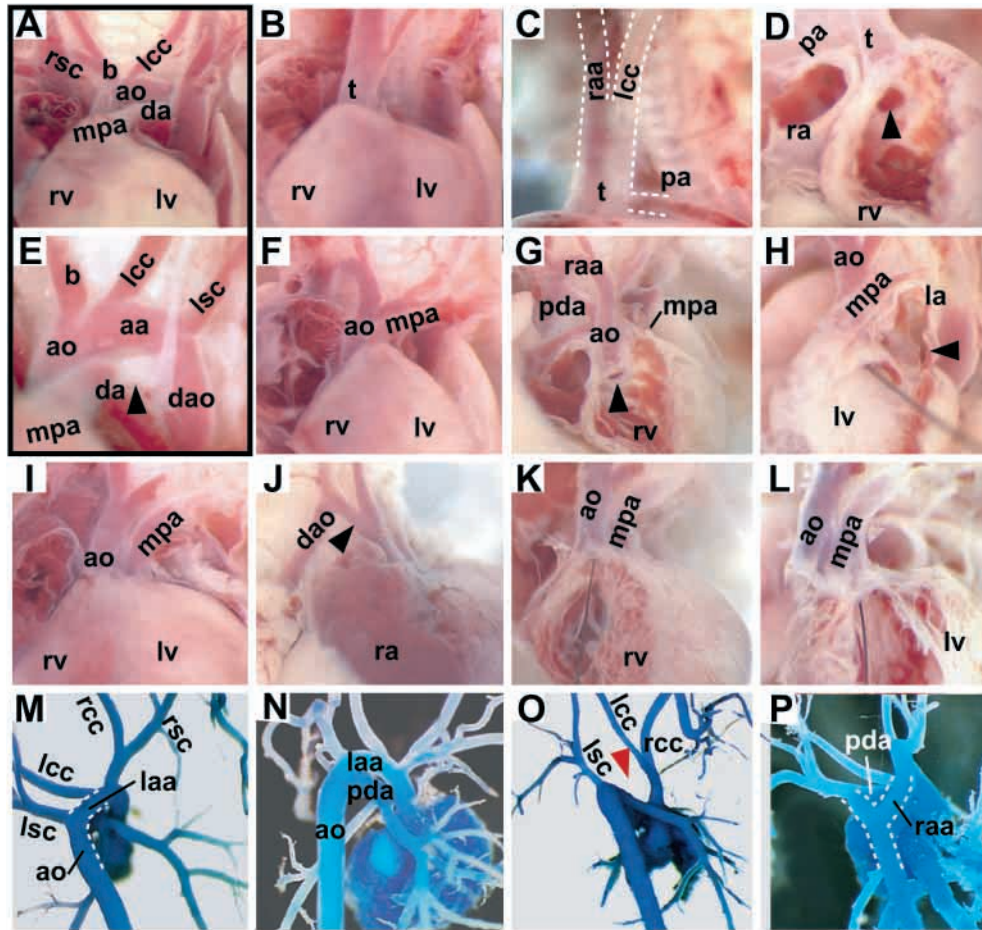
Fig. 2. E18.5 $Fgf8^{H/-}$ mutants exhibit lethal cardiovascular malformations. (A,E) Frontal and left oblique views of wild-type newborn heart and great vessels: the aorta (ao) arises from the left ventricle (lv) and is located to the right and posterior to the main pulmonary artery (mpa); the left aortic arch (aa) gives rise to the brachiocephalic (b), left common carotid (lcc) and left subclavian (lsc) and the aorta descends on the left (dao). The MPA arises from the right ventricle (rv). The ductus arteriosus (da) is closing (E, arrowhead). (B-D) Persistent Truncus Arteriosus results from failure of outflow tract septation. (B) Frontal view; a single vessel, the truncus (t), originates from the right ventricle (RV). (C) Left lateral view reveals origin of the left branch pulmonary artery (pa) and LCC from the truncal vessel. A right aortic arch was noted (raa). Broken lines have been superimposed to help clarify the anatomy. (D) Viewed from inside the RV, the truncal vessel overrides a large membranous ventricular septal defect (VSD, arrowhead), which is the only path of egress from the LV. The right atrium (ra) has been removed. (F-H) Double outlet right ventricle results from failure of outflow tract rotation and alignment. (F) Frontal view, MPA is anterior and towards the left of the aorta (Ao). (G) Right lateral view after removal of the right atrium and RV-free wall; note origins of Ao and MPA from the RV, there is a subaortic VSD (arrowhead), a right aortic arch and right patent ductus arteriosus (pda). (H) Left lateral view after removal of the LV free wall shows a probe passing from left ventricle through VSD into Ao; an atrial septal defect is visible from the left atrium (la, arrowhead). (I-L) D-Transposition of the great arteries results from failure of outflow tract rotation and alignment. (I) Frontal view; parallel circulation due to aberrant origin of the Ao anteriorly and from the RV and the MPA posteriorly from the LV. (J) Right lateral view shows right aortic arch (arrowhead), right descending aorta (dao) and right atrium (ra). (K) Right oblique view with probe passing from RV into Ao. (L) Left lateral view with probe passing from LV into MPA; there was no VSD. (M-P) Corrosion casts of the embryonic arterial vasculature reveal aortic arch anomalies in $Fgf8^{H/-}$ mutants. (M) Dorsal view of a control embryo; note continuity between ascending and descending aorta via the left aortic arch (laa), which is derived from the embryonic left fourth aortic arch artery. (N) Right dorsal oblique view of a control embryo; the PDA is visible, as is the LAA. (O) Posterior view of a mutant with interrupted aortic arch, type B; note discontinuity between ascending and descending aortas (red arrowhead) with the carotids arising from the ascending aorta and the left subclavian and descending aorta arising from the patent ductus arteriosus. (P) Dorsal oblique view of a mutant with a right aortic arch. A left-sided PDA and right aortic arch (raa) are shown. Broken lines have been superimposed to clarify the anatomy. This is a vascular ring encompassing the trachea and esophagus, which can cause airway obstruction and swallowing difficulties.

Histology, immunohistochemistry and TUNEL analysis of sections

Embryos were fixed in 4% paraformaldehyde (E9-E11.5) or Bouins fixative (E18.5). Paraffin embedded E9.5 to E11.5 embryos were sectioned at 5 μm and stained with a monoclonal antibody against Pecam-1 (1:50, Pharmingen), to label endothelial cells within the vasculature. A biotinylinated goat anti-rat secondary antibody (1:75, Pharmingen) was used and sections were developed in 3, 3′-diaminobenzidine with nickel chloride chromagen (Vector Laboratories) and counterstained with Eosin. E18.5 embryos were sectioned at 10 μm and stained with Hematoxylin and Eosin.

For cryosections, embryos were fixed in 4% paraformaldehyde and then protected in a sequential series of 10, 20 and 30% sucrose/PBS solutions, oriented in OCT (Tissue Tek) filled molds and rapidly frozen, then sectioned at 10 μm transversely with respect to neural tube and in parallel with the third pharyngeal arch. Sections were washed with PBS, blocked in 2% bovine serum albumin with 0.5% Triton-X100 and incubated overnight with primary antibodies: mouse monoclonal anti-AP2α (1:25, 3B5, Developmental Studies Hybridoma Bank), rabbit polyclonal anti-class III β-tubulin (1:500,Covance, α-Tuj1) or rabbit polyclonal antiphosphohistone H3 (1:100, Upstate Biotechnology, α-PHH3). Sections were washed, blocked and incubated with FITC conjugated anti-mouse IgG antibody (1:500, Molecular Probes), Cy-5 conjugated anti-rabbit IgG antibody (1:500, Jackson Laboratories), and TMR Red in situ cell death detection reagents (Roche). Sections were preserved in Vectashield anti-fading reagent (Vector Laboratories) and observed with confocal analysis at 20× magnification.
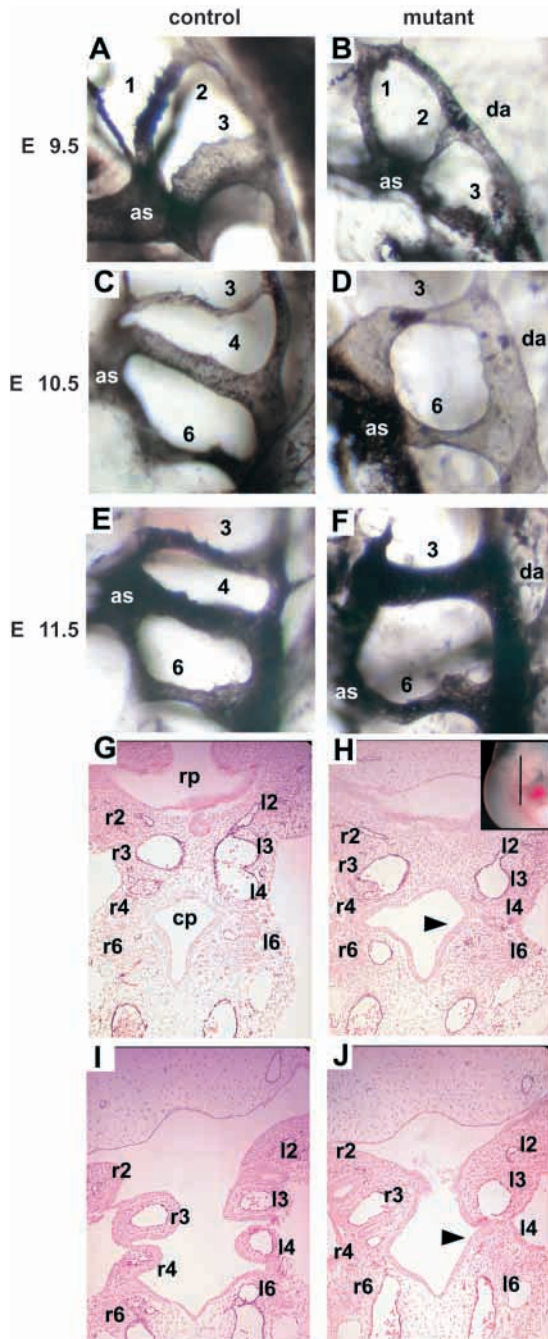
Fig. 3. Formation of the fourth pharyngeal arch arteries (PAAs) is abnormal in $Fgf8^{H/-}$ mutants. (A-F) Left lateral view after intracardiac ink injection to visualize the developing PAAs at E9.5 (A,B), 10.5 (C,D) and 11.5 (E,F) in $Fgf8$ mutants (B,D,F) and somite/stage matched controls (A,C,E). The PAAs are numbered and the aortic sac (as) and dorsal aorta (da) labeled. Note complete absence of the fourth PAAs in the mutants at E10.5 and E11.5, although the third and sixth PAAs are present. (G-J) Formation of the third pharyngeal pouch and fourth pharyngeal arch is disrupted in $Fgf8^{H/-}$ mutants. Immunohistochemistry for PECAM to stain the endothelium of the PAAs; plane of transverse sections through the arches is shown in inset of H. (G,I) control embryo, ventral (G) and dorsal (I); the ventral section is at the junction of the aortic sac with the origins of the second, third and fourth arch arteries. (H,J) Mutant embryo, ventral (H) and dorsal (J) transverse sections; the fourth pharyngeal arch tissue is hypoplastic, fused to the third arch and avascular on the left, although disorganized PECAM-positive endothelial cells are present (arrowheads); there is no third pouch on the left. The right fourth PAA is minimally endothelialized and never connects to the dorsal aorta (data not shown). The sixth arch arteries are larger than normal and have already fused with the dorsal aorta in section J. The rostral pharynx (rp) and caudal pharynx (cp) are labeled and the pharyngeal arches are numbered and labeled left (l) or right (r).

Alkaline phosphatase staining

Alkaline phosphatase staining of wholemounts was performed as previously described (Moon et al., 2000).

Whole-mount TUNEL analysis

Somite matched E9.5 embryos were fixed and subjected to Terminal UTP nick end labeling (TUNEL) as described elsewhere (Stadler et al., 2001). Confocal analysis was performed as above. Photomicrographs were taken at 8× magnification.

Fluorescent imaging

FITC, CY5, and Texas red fluorescence were recorded using a BioRad MRC 1024 laser-scanning confocal imaging system fitted to a Leitz Aristoplan microscope using filters supplied by the manufacturer. A digital Kalman averaging filter was used to reduce background fluorescence.

RESULTS

Compound heterozygous mice bearing hypomorphic and null alleles of *Fgf8* produce less *Fgf8* mRNA than controls and display lethal malformations
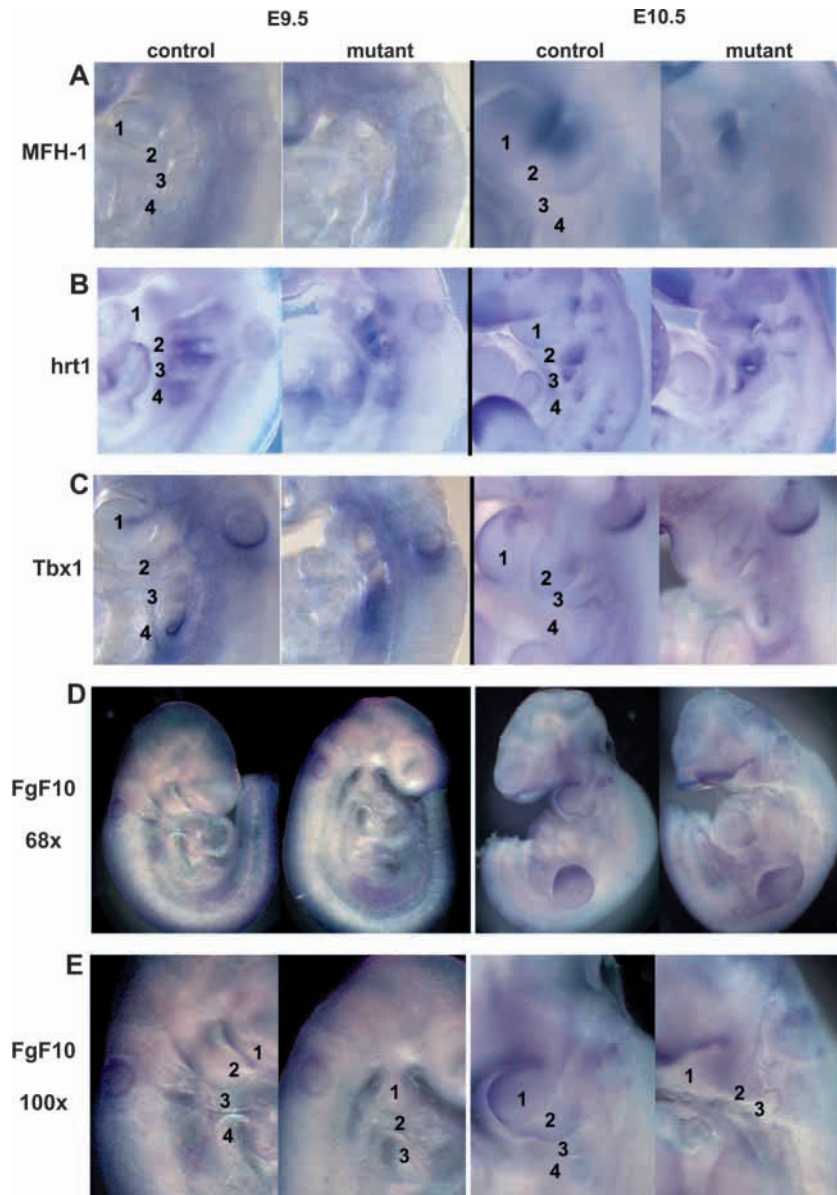
In order to bypass embryonic lethality resulting from complete ablation of $Fgf8$ function in embryonic mice, we investigated the role of $Fgf8$ in cardiovascular and pharyngeal arch development with a hypomorphic allele. The $Fgf8^H$ allele contains a neomycin phosphotransferase (neo^r) and alkaline phosphatase reporter genes in the 3′ untranslated region of an otherwise intact $Fgf8$ locus (Fig. 1A). This has significant transcriptional consequences. Quantitative RT-PCR amplification (Fig. 1B), reveals that compound heterozygotes bearing hypomorphic ($Fgf8^H$) and null ($Fgf8^-$) alleles of $Fgf8$ ($Fgf8^{H/-}$, henceforth called mutants), reproducibly generate less $Fgf8$ mRNA, when compared with control littermates. The decreased function of the hypomorphic relative to the wild-type allele clear if one compares the compound heterozygotes

Whole-mount in situ hybridization

In situ hybridization on intact embryos was carried out as previously described (Moon et al., 2000). The plasmids used to generate riboprobes were generously provided by N. Miura (mfh-1), B. Morrow (tbx-1), D. Srivastava (hrt-1) and D. Ornitz (Fgf10).

Flow cytometry

Thymocytes from embryos at 18.5 days of gestation were dispersed through nylon mesh into PBS, washed, counted on a hemocytometer using Trypan Blue to exclude non-viable cells, stained for cell surface markers (PE-anti-CD25, PerCP-anti-CD8, APC-anti-CD4, FITC-anti-CD44 from PharMingen), washed, resuspended in PBS and analyzed by flow cytometry on a FACSCaliber® (Becton Dickinson).

Fig. 4. Mesenchymal expression of *Fgf10* is decreased, while *Mfh1*, *Hrt1* and *Tbx1* appear normal in *Fgf8*[H/−] mutants. Views of the pharyngeal arch area, head is at the top. Arches are numbered in the controls. (A) *Mfh1*, (B) *Hrt1*, (C) *Tbx1* and (D,E) *Fgf10* expression in E9.5 and E10.5 control and mutant embryos. (E) Note the markedly decreased signal in the pharyngeal arches, including area of the developing fourth arch and putative secondary heart field, although expression in limb bud and ototcyst is relatively intact.

abnormalities are present in all of these animals: 100% have micrognathia and 30% have bony cleft palate (Fig. 1D); other facial malformations such as fusion of the temporomandibular joint and absence of the tympanic ring are more variable within and between mutants. Central nervous system malformations are seen in all mutants including hypoplasia or aplasia of the cerebellum and olfactory bulbs (data not shown). These phenotypes reflect dose sensitivity for FGF8 because *Fgf8*^{+/−} null allele heterozygotes (which produce approximately 50% the wild type amount of *Fgf8* mRNA) and *Fgf8*[+/H] hypomorph allele heterozygotes (which produce a quantity intermediate to that of wild type and null heterozygotes) are normal.

Fgf8[H/−] mice die from congenital cardiovascular defects

Multiple, severe developmental defects contribute to the neonatal demise of some mutants; however, most die a cardiovascular death, with progressive cyanosis and respiratory failure. We discovered cardiovascular defects in 95% of 60 term mutants, most of which were lethal malformations (Fig. 2, summarized in Table 1).

Outflow tract septation, rotation and alignment defects were common in these mutants. Persistent truncus arteriosus was the

(in which the only source of *Fgf8* mRNA is the *Fgf8*[H] allele) and null heterozygotes (in which only the *Fgf8*^{+} allele produces *Fgf8* mRNA). We have previously shown that removal of the neo[r] gene from the *Fgf8*[H] allele restores its function (Moon and Capecchi, 2000).

Decreased production of *Fgf8* mRNA has important phenotypic consequences. *Fgf8*[H/−] mutants are small and die as neonates with cyanosis, respiratory distress, edema and multiple congenital anomalies (Fig. 1C). Craniofacial

most embryologically primitive lesion observed and results from complete failure of septation of the primitive truncal vessel to form the ascending aorta and main pulmonary artery. Instead, the branch pulmonary arteries, the great vessels of the head and neck, and the descending aorta all arise from a single vessel (Fig. 2B-D). Transposition of the great arteries is a defect in which the aorta arises abnormally from the right ventricle and the pulmonary artery from the left ventricle (inverted ventriculo-arterial alignment, Fig. 2I-L). After birth

Table 1. Incidence of congenital cardiovascular lesions in *Fgf8*[H/N] mutants

Defect	IAAB	TA	VSD	TGA	DORV/TOF	RAA	SC	RPA	Normal
Number (60 in total)	14	4	33	21	12	36	46	2	2
%	24	7	55	36	21	60	78	3	3

IAAB, interrupted aortic arch type B; TA, truncus arteriosus; VSD, ventricular septal defect; TGA, transposition of the great vessels; DORV/TOF, double outlet right ventricle/tetralogy of Fallot; RAA, right aortic arch; SC, abnormal subclavian branching, including aberrant right and/or left subclavian arteries; RPA, right pulmonary isomerism.

and upon the closure of the ductus arteriosus, two parallel circulations form such that the systemic circulation is deprived of oxygen and death rapidly ensues. Double outlet right ventricle (Fig. 2F-H) and Tetralogy of Fallot (overriding aorta, ventricular septal defect, pulmonary stenosis and hypertrophy of the right ventricle) are more complex rotation/alignment defects that were observed.

Vascular defects were observed in the majority of mutants (see Table 1) and included interrupted aortic arch type B, in which the arch of the aorta fails to form between the left common carotid artery and left subclavian artery (IAAB, Fig. 2O); right aortic arch (Fig. 2P); and anomalous origin of the subclavian arteries. These defects indicate that formation, stabilization or remodeling of the fourth PAAs is disrupted in the mutants. The right and left fourth PAAs form between E 9.5-E10.0. The right fourth PAA gives rise to the origin of the right subclavian artery. The left fourth PAA becomes the arch of the aorta between the left common carotid artery and left subclavian artery which is the portion of the aorta that is absent in IAAB.

To evaluate fourth PAA formation, we performed intravascular ink injections in E9.5 to E 11.5 mutants and controls. At E9.5, prior to the formation of the fourth PAA, mutant animals have patent PAAs 1-3, as do controls (Fig. 3A,B). The fourth PAA is not patent to ink injection in E10.0 to E11.5 mutants (Fig. 3C-F). All mutants display abnormal fourth PAA formation bilaterally at E10.5 (Table 2). The absence of these arteries can not be attributed to growth delay, as the sixth PAA is present by E10-10.5 (Fig. 3D,F,H,J). A mutant sectioned coronally through the pharyngeal arches and immunohistochemically stained with the endothelial marker PECAM demonstrates that endothelial cells can be detected in the left fourth arch region, although they are disorganized and no vessel lumen is evident (Fig. 3H, left side). On the right-hand side of this animal, the right fourth vessel appears patent in the section displayed, but serial sections revealed that it never connected with the dorsal aorta.

At E10.5, mutants frequently had hypoplastic fourth pharyngeal arch tissue fused to the third arch and no third pouch (Fig. 3H,J). In combination with the vascular defects reported above, this finding suggests that formation of the fourth arch itself and patterning of the third and fourth arches may be disrupted. To determine if decreased FGF8 in the mutants altered expression of transcription factors expressed during fourth arch development, we performed whole mount in situ hybridization in E9.5 and E10.5 embryos. *Mfh1* (*Foxc2* – Mouse Genome Informatics) encodes a winged helix transcription factor that has been shown to be expressed in the pharyngeal arch vessels and mesenchyme from E9.5; ablation of *Mfh1* function results in interrupted aortic arch type B due to aberrant remodeling of the fourth PAA (Iida et al., 1997). *Mfh1* expression appeared normal in *Fgf8* mutants (Fig. 4A)

Expression of *Hrt1*, which encodes a basic helix-loop-helix transcription factor expressed in the developing arch mesenchyme and endoderm and is a downstream mediator of Notch signaling (Nakagawa et al., 2000; Nakagawa et al., 1999), also appeared normal in *Fgf8* mutants (Fig. 4B).
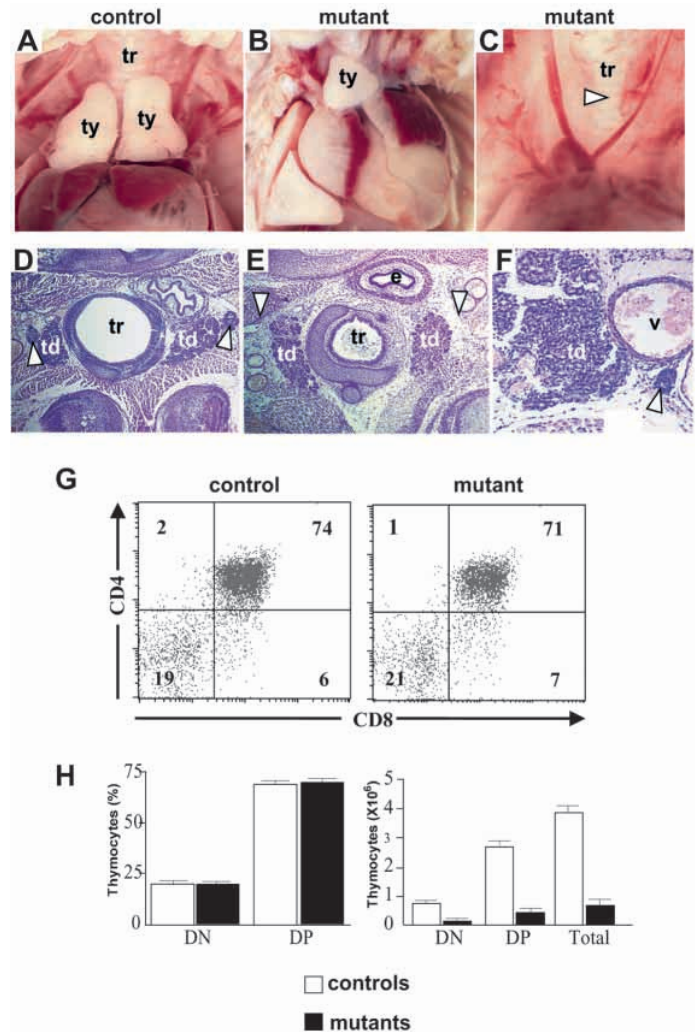

Fig. 5. *Fgf8*[H/−] mutants display glandular phenotypes and T-cell deficiency attributable to altered pharyngeal pouch development. eighty percent of mutants had thymic (Ty) hypo/aplasia and 50% had parathyroid hypo/aplasia. (A-C) Thoracotomies, (D-F) Hematoxylin and Eosin stained paraffin wax-embedded sections. The trachea (tr), esophagus (e) and thyroids (td) are also indicated. (A) Normal bi-lobed thymus in a control E18.5 embryo. (B) Hypoplastic, mono-lobed thymus in a mutant. (C) Thymic aplasia in a mutant (arrowhead). (D) Normal bilateral parathyroid glands in a control E18.5 embryo (arrowheads). (E) Parathyroid aplasia in a mutant (arrowheads), the entire cervical region of this animal was sectioned and no parathyroids were detected. (F) Ectopic, hypoplastic parathyroid (arrowhead) adjacent to internal carotid vessel (v) in a mutant. (G) Representative FACS plots of control and mutant thymi. (H) Percent (left panel) and total (right panel) CD4−CD8−double negative (DN) and CD4+CD8+double positive (DP) thymocytes in *n*=9 control embryos or *n*=2 mutant embryos with thymic hypoplasia. Mutants with thymic hypoplasia have 20% of the normal number of T cells. Note that 50% of mutant embryos have no thymus. Data are shown as mean±s.e.m.
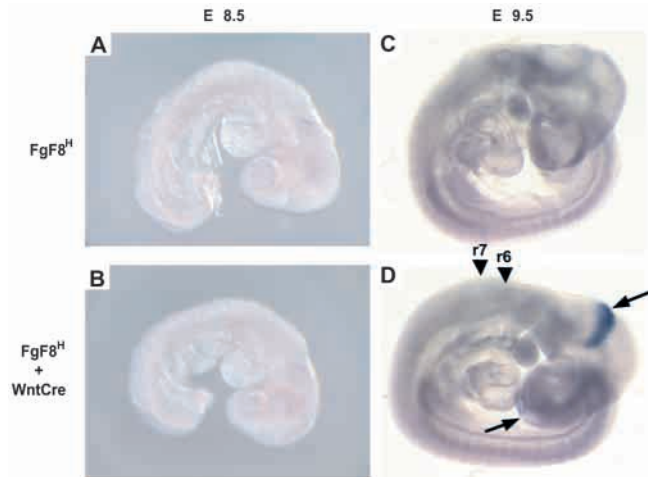
Table 2. Failure of formation of the fourth pharyngeal arch artery in *Fgf8*[H/N] mutants

	Fourth PAA	Right	Left
Control (*n*=9)	Normal	100%	100%
Mutant (*n*=9)	Normal	None	None
	Small/atretic	44%	33%
	Absent	56%	67%

Fig. 6. Premigratory and migratory cardiac and pharyngeal neural crest do not express *Fgf8*. *Wnt1*-Cre was used to drive expression of the alkaline phosphatase (AP) reporter gene from the *Fgf8*^H allele in premigratory and migrating neural crest; Cre-mediated recombination of the *Fgf8*^H allele results in expression of the AP gene regulated by the *Fgf8* promoter and is detected as blue staining. (A) E8.5 control embryo bearing the *Fgf8*^H allele. (B) E8.5 embryo bearing the *Fgf8*^H and the *Wnt1*-Cre transgene; no staining is detected, indicating that *Fgf8* is not expressed in any cells of the *Wnt1-Cre* lineage at this stage. (C) E9.5 control embryo with the *Fgf8*^H allele. (D) E9.5 embryo bearing the *Fgf8*^H allele and the *Wnt1-Cre* transgene; blue staining reveals overlapping domains of *Wnt1* and *Fgf8* expression in the isthmus and frontonasal prominences (arrows). No activity in neural crest of rhombomeres 6-8 (R6, R7 arrowheads), which are the origin of premigratory third and fourth pharyngeal and cardiac neural crest.

Although *Fgf8*^H/− and *Tbx1* mutants have overlapping phenotypes and are both genes are expressed in the pouch endoderm, we did not detect any change in the pattern of *Tbx1* expression at these stages (Fig. 4C).

We have previously shown that ectodermal FGF8 maintains mesenchymal *Fgf10* expression in the developing limb bud and questioned whether a similar relationship occurred between FGF8 and *Fgf10* in the pharyngeal arch epithelia and mesenchyme (Moon and Capecchi, 2000). Examination of *Fgf10* expression at E9.5 and E10.5 (Fig. 4D,E) revealed markedly decreased signal in the pharyngeal arch mesenchyme, including the regions of the developing fourth arch and putative secondary heart field (Kelly et al., 2001).

Fgf8^H/− mice exhibit thymic and parathyroid aplasia and hypoplasia

The thymus and parathyroid glands develop from the third and fourth pharyngeal pouch endoderm and migrate caudally to their final location in the mediastinum. We analyzed mutants by gross dissection and in sections, and found that 50% of mutants had no detectable thymus, while in another 50% the thymus was hypoplastic with small single or double lobes or strands of thymic tissue ectopically located in the rostral region of the neck (Fig. 5A-C). Rarely, ectopic thymic tissue could be found penetrating into the oropharynx of E18.5 mutants (data not shown). The parathyroid glands were aplastic or hypoplastic in 50% of mutants (Fig. 5D-F).

Fgf8 mutants have a T-cell deficiency

One of the cardinal features of individuals with deletion 22q11 and DiGeorge sequence is a variable immunodeficiency associated with decreased number of T cells (Jawad et al., 2001). Though 50% of the *Fgf8* mutants had aplasia of the thymus, we were able to evaluate T cells in those with hypoplastic glands. Fig. 5G shows representative FACS (fluorescence activated cell sort) plots comparing T cells obtained from control and mutant thymi immunostained with anti CD4 and anti CD8 antibodies. In Fig. 5H, the percent (left panel) and total (right panel) number of CD4−CD8−double negative (DN) and CD4+CD8+double positive (DP) thymocytes are compared in E18.5 controls and mutants; mutants had 20% of the normal number of T cells. The thymocyte subpopulations were normal and no difference was detected in CD44 or CD25 staining of double negative-gated thymocytes (data not shown).

Fgf8 is not expressed in neural crest cells

The *Fgf8*^H/− mutant phenotypes are striking in their similarity to human del22q11 syndromes and animal models of neural crest dysfunction. Although *Fgf8* expression has not been reported in neural crest in the mouse, it is possible that these defects arise from a deficiency of FGF8 in a previously undetected expression domain in neural crest. To determine if *Fgf8* is expressed in premigratory or migratory neural crest, we combined the *Wnt1*-Cre transgene (Jiang et al., 2000) with the alkaline phosphatase (AP) reporter/conditional features of the *Fgf8*^H allele (Moon and Capecchi, 2000) (Fig. 1A). LoxP sites flank exon 5 and neo^r, and enable conditional expression of the AP reporter upon Cre-mediated recombination of the *Fgf8*^H allele. In this experiment, cells of the *Wnt1* lineage, including premigratory cardiac neural crest (Echelard et al., 1994), contain the recombined *Fgf8*^H allele; thus, blue AP staining indicates cells that currently or previously express(ed) *Wnt1*, and that currently express *Fgf8* (Fig. 6). We detected overlapping domains of *Wnt1* and *Fgf8* expression in the isthmus and frontonasal prominences at E9.5 (Crossley and Martin, 1995; Echelard et al., 1994), but none in the domain of premigratory or migratory cardiac neural crest, which originates in rhombomeres six through eight, at either E8.5 or E9.5. These results suggest that the cardiovascular and glandular phenotypes of *Fgf8* mutants result from altered signaling between the pharyngeal epithelium, the mesodermal mesenchyme, and neural crest en route to the arches, outflow tract and heart.

Pharyngeal and cardiac neural crest undergoes abnormal apoptosis in *Fgf8*^H/− mice

We questioned whether neural crest survival and migration were affected by decreased FGF8 in the pharyngeal ectoderm and endoderm of the pharyngeal arches. Using whole-mount TUNEL analysis, we found an increased number of apoptotic cells and abnormal domains of apoptosis in the pharyngeal arches of mutants when compared with controls (Fig. 7A-C). The expression of *Fgf8* is also shown to help the reader visualize how the apoptotic domains relate spatially to regions of *Fgf8* expression (Fig. 7D-F). Note that there are domains of apoptosis adjacent and relatively distant to locations of normal FGF8 signaling.

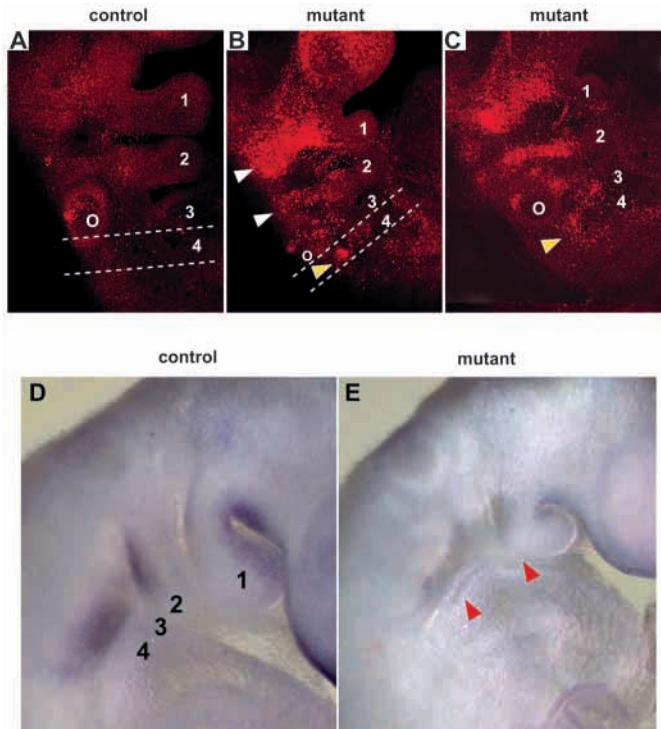To determine specifically if abnormal apoptosis was

Fig. 7. There is increased apoptosis in the pharyngeal arches of *Fgf8*[H/−] mutants in domains adjacent and remote to *Fgf8* expression. Whole mount TUNEL analysis was performed on 25 somite, stage-matched control. (A) and mutant (B,C) embryos. Pharyngeal arches are numbered and the otocyst is labeled (O); note the increased number of apoptotic cells in normal domains in the rostral arches (white arrowheads in B) and abnormal domains of apoptosis in the postotic region of the developing fourth and sixth arches (yellow arrowheads) in the mutants. *Fgf8* expression by in situ hybridization on E9.5 control and mutant embryos. (D,E) Pharyngeal region of control embryo and (E) mutant embryo; note severely decreased quantity of *Fgf8* message in the mutant (red arrowheads, consistent with results in Fig. 1B). Domains of apoptosis in B and C are seen both adjacent, and relatively distant, to normal regions of *Fgf8* expression.

occurring in neural crest, we performed fluorescent immunohistochemistry using anti-AP-2α antibody to label migrating neural crest in cryosectioned embryos (Mitchell et al., 1991). Domains of apoptosis in the neural tube and developing ganglia were present in mutants and controls at the 25 somite stage (Fig. 8A,B, blue arrowheads), but the domains were much larger in the mutants (Fig. 8, yellow arrowheads). In the mutants, there were additional abnormal domains of apoptosis and many TUNEL/antiAP-2α double-labeled cells (yellow signal, yellow arrowheads) in neural crest migrating from rhombomeres 6 and 7 into the lateral developing fourth and sixth arches. This finding was reproducible and persisted to the 29 somite stage (Fig. 8C,D). No reproducible differences in proliferation were detected at this stage, as assayed with an antiphosphohistone H3 antibody to label chromatin in proliferating cells. Note that in whole-mount TUNEL and cryosectioned specimens, many of the apoptotic cells are distant from the sources of FGF8 in the pharyngeal pouches and clefts shown in Fig. 7 (Crossley and Martin, 1995; Heikinheimo et al., 1994; MacArthur et al., 1995).

DISCUSSION

We have described an *Fgf8* hypomorphic mouse that displays a range of pharyngeal and cardiovascular phenotypes that closely phenocopies human del22q11 syndrome. We postulate that these developmental defects result from an insufficient dosage of FGF8 locally in the pharyngeal arches. The fact that both *Fgf8*[+/H] and *Fgf8*^{+/−} heterozygotes are normal indicates that a crucial decrease in the dose of FGF8 occurs when the hypomorphic and null alleles are combined in a single embryo. If the phenotypes were due to an effect of the neo[r] gene on other loci, *Fgf8*[+/H] heterozygotes would be affected. Furthermore, ablation of *Fgf8* function in the pharyngeal arch ectoderm using a tissue-specific Cre recombinase and a nonhypomorphic conditional allele reproduces many features of the phenotype (Arenkiel and Moon, unpublished data) and reveals that the roles of FGF8 in left-right specification (Meyers and Martin, 1999) and in pharyngeal and cardiovascular development are separable. Meyers and colleagues have previously described aberrant *Fgf8* splicing into a neo[r] gene targeted to an intron that resulted in a hypomorphic allele (Meyers et al., 1998); this hypomorphic affect appears to be significantly more severe than that resulting from placement of neo[r] in the 3′UTR that we describe. They described a range of defects in their compound heterozygotes including early embryonic death, gastrulation failure, severe CNS malformations and left-right asymmetry defects, which indicates earlier and more severe FGF8 deficiency in these animals (Meyers et al., 1998; Meyers and Martin, 1999). Our *Fgf8*[H/−] mice have focal developmental defects from reduced FGF8 dose, indicating that this hypomorphic allele produces sufficient functional *Fgf8* message for the embryo to gastrulate and specify the left-right axis correctly. The work of both groups reveals that different tissues have different dosage requirements for FGF8 likely reflecting redundancy other FGFs (Moon et al., 2000; Moon and Capecchi, 2000; Lewandoski et al., 2000; Sun et al., 2000).

Deficiency of FGF8 causes cardiovascular, craniofacial and glandular phenotypes resulting from abnormal pharyngeal arch development, altered mesenchymal expression of *Fgf10* and decreased neural crest survival. Similar to our observation in the developing limb (Moon and Capecchi, 2000), we found that epithelial FGF8 is required for expression of *Fgf10* in the pharyngeal arch mesenchyme, including the region of the developing fourth pharyngeal arch and the putative secondary heart field (Kelly et al., 2001). Further experiments will be required to determine if aspects of the outflow tract defects seen in *Fgf8* hypomorphs are related to this finding. Tissue-specific ablation of FGF8 in the pharyngeal epithelia may clarify its role in this region.

Although cardiac neural crest does not itself express *Fgf8*, *Fgf8* mutants display increased apoptosis in this tissue, indicating that FGF8 signaling from pouch endoderm and ectoderm is important for its survival. FGF receptors are expressed in the ectoderm and throughout the mesenchyme of the pharyngeal arches (MacArthur et al., 1995; Orr-Urtreger et al., 1993; Orr-Urtreger et al., 1991; Peters et al., 1992). Our whole-mount TUNEL and analysis of apoptosis in sections reveals that some of the apoptosis is (not surprisingly) directly adjacent to sites of epithelial *Fgf8* expression (Crossley and Martin, 1995; Heikinheimo et al., 1994; MacArthur
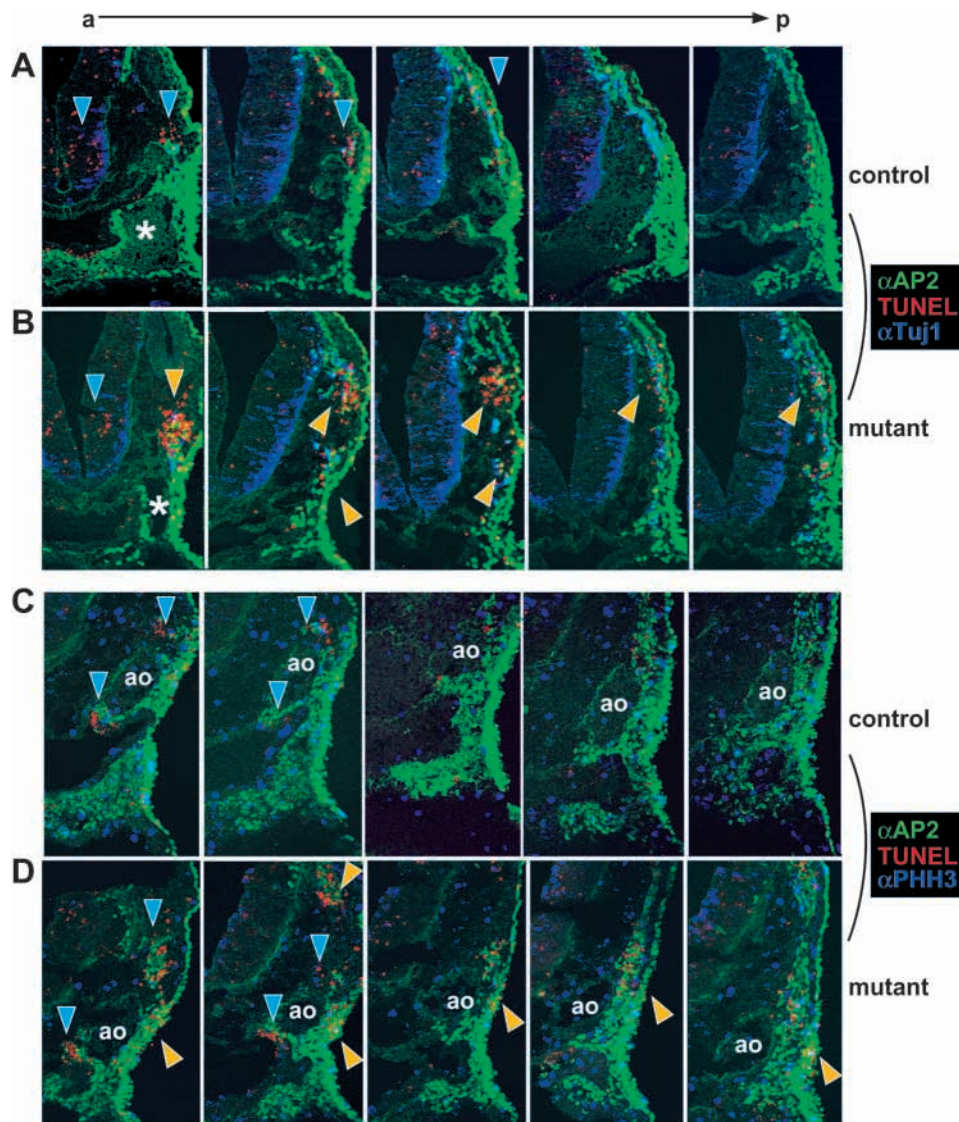
Fig. 8. Migrating cardiac neural crest undergoes abnormal apoptosis in *Fgf8*[H/−] mutants. Fluorescent immunohistochemistry was performed on transverse cryosections using a combination of anti-AP-2/FITC (green), TUNEL/Texas red (red) and either (A,B) anti-Tuj1/Cy5 (blue) which labels neuronal tubulin, or (C,D) antiPHH3/Cy5 (blue), which labels chromatin in proliferating cells. (A,B) Twenty-five somite stage matched (A) control and (B) mutant; plane and region of sections are illustrated by broken lines in Fig. 7B. White asterisks mark the third PAA in parallel. (C,D) Twenty-nine somite stage matched (C) control and (D) mutant; sections begin just posterior to the junction of the third aortic arch artery with the dorsal aorta (ao). From left to right, sections proceed from anterior to posterior through the post-otic region. Blue arrowheads indicate normal domains of apoptosis, including regions of developing ganglia and neural tube that label with anti-Tuj1. Yellow arrowheads indicate increased numbers of apoptotic cells in normal domains or abnormal domains of apoptosis in mutant neural crest mesenchyme. Yellow staining indicates double labeling of cardiac/pharyngeal neural crest cells with anti-AP-2α and TUNEL, and reveals abnormal apoptosis in lateral neural crest of the developing fourth arch. No reproducible differences in PHH3 staining were detected at this stage.

et al., 1995) (Fig. 7) and probably reflects the failure of FGF8/FGFR1- or FGF8/FGFR2-mediated signaling. However, other large domains of mesenchymal apoptosis are relatively distant from these sources. This finding suggests that altered FGF8 signaling is sensed or relayed distant to its expression domains; such relays may, or may not, be based on FGF/FGFR interactions. We have reported the same phenomenon in proximal limb mesenchyme after conditional ablation of FGF8 in the distal limb ectoderm (Moon and Capecchi, 2000) and reproduced this finding after ablation of both FGF4 and FGF8 in the limb ectoderm (A. M. Boulet, M. R. C. and A. M. M., unpublished). Ablation of FGF8 in first arch ectoderm results in abnormal apoptosis of neural crest-derived mesenchyme (much of which is distant to the epithelial FGF8 source (Trumpp et al., 1999), similar to that described here.

The phenotypes of *Fgf8* and *Tbx1* mutants confirm that pharyngeal endoderm plays a crucial role in patterning the pharyngeal neural crest and mesoderm-derived mesenchyme (Couly et al., 2002; LeDouarin, 1982; Piotrowski and Nusslein-Volhard, 2000; Thomas et al., 1998; Veitch et al., 1999; Wendling et al., 2000). The importance of cardiac neural crest in the pathogenesis of the human del22q11 syndromes is supported by neural crest ablations in chick (Creazzo et al., 1998) and the *splotch* mouse (Conway et al., 1997b; Epstein et al., 2000). Several mouse models with neural crest dysfunction exhibit conotruncal and aortic arch defects (Bamforth et al., 2001; Feiner et al., 2001; Mendelsohn et al., 1994; Schorle et al., 1996; Zhang et al., 1996). Our results concur with accumulating evidence that neural crest cells rely on signals from adjacent tissues for patterning and survival en route to their targets (Trainor and Krumlauf, 2000) and indicate an important role for epithelial-mesenchymal interactions in neural crest function during development.

Aortic arch abnormalities arise from defects in formation or remodeling of the PAAs, although models vary considerably in pathogenesis. In neural crest-ablated chicks, PAA 3, PAA 4 and PAA 6 are formed but rapidly regress (Kirby, 1999). This indicates that interactions between neural crest, the primitive vessel and possibly the mesodermal mesenchyme are required for stabilization and subsequent remodeling of the vessel. In *Df1* heterozygotes or *Tbx1* haploinsufficient mice, the fourth PAA is specifically affected. These mutants initially form an

endothelialized tube that is not stabilized and by E10.5, 100% of animals have a nonpatent vessel (Lindsay and Baldini, 2001; Lindsay et al., 1999; Lindsay et al., 2001). Recovery from this defect is variable resulting in a 30% incidence of primarily right-sided cardiovascular defects. Homozygous mutants of *Crkol*, *Mfh1* or genes in the endothelin signaling pathway all demonstrate fourth PAA defects in which arteries form normally, but regress to a variable extent after E11.5 (Guris et al., 2001; Iida et al., 1997; Kurihara et al., 1995; Yanagisawa et al., 1998). Our *Fgf8* mutants exhibit early defects in vessel formation and stabilization similar to the *Tbx1* and *Df1* mutants described by Lindsay and colleagues (Lindsay and Baldini, 2001; Lindsay et al., 1999; Lindsay et al., 2001). Endothelial cells are aggregated in the fourth arch at E10.5, but patent vessel lumens are not evident. However, we see a greater proportion of left sided and bilateral defects at E10.5, and no evidence of recovery by E11.5. This results in a greater incidence of fourth PAA defects in the newborns, particularly the more severe left-sided phenotypes of IAAB and right aortic arch.

The *Fgf8* hypomorphic phenotype suggests that *Fgf8* may contribute to the variability of human del22q11 phenotypes as a modifier, or may be a causative locus in syndromic individuals that do not have deletions of 22q11. Complete inactivation of one allele of *Fgf8* in conjunction with a decrease in function of the remaining allele in mice provides a spectrum of disease closely resembling that seen in humans. FGF8 may participate directly in molecular pathways affected by deletions in the 22q11 region or function in parallel pathways required for normal development of pharyngeal arch and neural crest-derived tissues.

Given the lack of genotype-phenotype correlation in humans with the 22q11 deletion, it is possible that dysfunction of other developmentally active loci is required to produce the most severe del22q11 phenotypes. To test this hypothesis in mice, we are searching for genetic interactions by evaluating mice bearing combinations of mutant loci known to generate aspects of this phenotype. Screening individuals with del22q11 for mutations on the nondeleted chromosome 22 or for mutations in genes known to contribute to pharyngeal arch development (*Fgf8*, *Pax3*, for example) will provide another important test of this hypothesis.

REFERENCES

Bamforth, S. D., Braganca, J., Eloranta, J. J., Murdoch, J. N., Marques, F. I., Kranc, K. R., Farza, H., Henderson, D. J., Hurst, H. C. and Bhattacharya, S. (2001). Cardiac malformations, adrenal agenesis, neural crest defects and exencephaly in mice lacking Cited2, a new Tfap2 co-activator. *Nat. Genet.* **29**, 469-474.

Birgbauer, E., Sechrist, J., Bronner-Fraser, M. and Fraser, S. (1995). Rhombomeric origin and rostrocaudal reassortment of neural crest cells revealed by intravital microscopy. *Development* **121**, 935-945.

Bockman, D. E. and Kirby, M. L. (1984). Dependence of thymus development on derivatives of the neural crest. *Science* **223**, 498-500.

Bockman, D. E., Redmond, M. E. and Kirby, M. L. (1989). Alteration of early vascular development after ablation of cranial neural crest. *Anat. Rec.* **225**, 209-217.

Burn, J., Takao, A., Wilson, D., Cross, I., Momma, K., Wadey, R., Scambler, P. and Goodship, J. (1993). Conotruncal anomaly face syndrome is associated with a deletion within chromosome 22q11. *J. Med. Genet.* **30**, 822-824.

Chieffo, C., Garvey, N., Gong, W., Roe, B., Zhang, G., Silver, L., Emanuel, B. S. and Budarf, M. L. (1997). Isolation and characterization of a gene from the DiGeorge chromosomal region homologous to the mouse Tbx1 gene. *Genomics* **43**, 267-277.

Conway, S. J., Henderson, D. J. and Copp, A. J. (1997a). Pax3 is required for cardiac neural crest migration in the mouse: evidence from the splotch (Sp2H) mutant. *Development* **124**, 505-514.

Conway, S. J., Henderson, D. J., Kirby, M. L., Anderson, R. H. and Copp, A. J. (1997b). Development of a lethal congenital heart defect in the splotch (Pax3) mutant mouse. *Cardiovasc. Res.* **36**, 163-173.

Couly, G., Creuzet, S., Bennaceur, S., Vincent, C. and le Douarin, N. M. (2002). Interactions between Hox-negative cephalic neural crest cells and the foregut endoderm in patterning the facial skeleton in the vertebrate head. *Development* **129**, 1061-1073.

Creazzo, T. L., Godt, R. E., Leatherbury, L., Conway, S. J. and Kirby, M. L. (1998). Role of cardiac neural crest cells in cardiovascular development. *Annu. Rev. Physiol.* **60**, 267-286.

Crossley, P. H. and Martin, G. R. (1995). The mouse Fgf8 gene encodes a family of polypeptides and is expressed in regions that direct outgrowth and patterning in the developing embryo. *Development* **121**, 439-451.

Dietrich, S. and Gruss, P. (1995). undulated phenotypes suggest a role of Pax-1 for the development of vertebral and extravertebral structures. *Dev. Biol.* **167**, 529-548.

DiGeorge, A. M. (1965). Discussion on a new concept of the cellular basis of immunology. *J. Pediatr.* **67**, 907.

Echelard, Y., Vassileva, G. and McMahon, A. P. (1994). Cis-acting regulatory sequences governing Wnt-1 expression in the developing mouse CNS. *Development* **120**, 2213-2224.

Emanuel, B. S., McDonald-McGinn, D., Saitta, S. C. and Zackai, E. H. (2001). The 22q11.2 deletion syndrome. *Adv. Pediatr.* **48**, 39-73.

Epstein, J. A., Li, J., Lang, D., Chen, F., Brown, C. B., Jin, F., Lu, M. M., Thomas, M., Liu, E., Wessels, A. et al. (2000). Migration of cardiac neural crest cells in Splotch embryos. *Development* **127**, 1869-1878.

Etchevers, H. C., Couly, G., Vincent, C. and le Douarin, N. M. (1999). Anterior cephalic neural crest is required for forebrain viability. *Development* **126**, 3533-3543.

Feiner, L., Webber, A. L., Brown, C. B., Lu, M. M., Jia, L., Feinstein, P., Mombaerts, P., Epstein, J. A. and Raper, J. A. (2001). Targeted disruption of semaphorin 3C leads to persistent truncus arteriosus and aortic arch interruption. *Development* **128**, 3061-3070.

Franz, T. (1989). Persistent truncus arteriosus in the Splotch mutant mouse. *Anat. Embryol.* **180**, 457-464.

Garg, V., Yamagishi, C., Hu, T., Kathiriya, I. S., Yamagishi, H. and Srivastava, D. (2001). Tbx1, a DiGeorge syndrome candidate gene, is regulated by sonic hedgehog during pharyngeal arch development. *Dev. Biol.* **235**, 62-73.

Gottlieb, S., Driscoll, D. A., Punnett, H. H., Sellinger, B., Emanuel, B. S. and Budarf, M. L. (1998). Characterization of 10p deletions suggests two nonoverlapping regions contribute to the DiGeorge syndrome phenotype. *Am. J. Hum. Genet.* **62**, 495-498.

Goulding, M., Sterrer, S., Fleming, J., Balling, R., Nadeau, J., Moore, K. J., Brown, S. D., Steel, K. P. and Gruss, P. (1993). Analysis of the Pax-3 gene in the mouse mutant splotch. *Genomics* **17**, 355-363.

Guris, D. L., Fantes, J., Tara, D., Druker, B. J. and Imamoto, A. (2001). Mice lacking the homologue of the human 22q11.2 gene CRKL phenocopy neurocristopathies of DiGeorge syndrome. *Nat. Genet.* **27**, 293-298.

Heikinheimo, M., Lawshe, A., Shackelford, G. M., Wilson, D. B. and MacArthur, C. A. (1994). Fgf-8 expression in the post-gastrulation mouse suggests roles in the development of the face, limbs and central nervous system. *Mech. Dev.* **48**, 129-138.

Herve, J., Warnet, J. F., Jeaneau-Bellego, E., Portnoi, M. F., Taillemitte, J. L. and Herve, F. (1984). Partial monosomy of the short arm of chromosome 10, associated with Rieger's syndrome and a Di George type partial immunodeficiency. *Ann. Pediatr.* **31**, 77-80.

Iida, K., Koseki, H., Kakinuma, H., Kato, N., Mizutani-Koseki, Y.,

Ohuchi, H., Yoshioka, H., Noji, S., Kawamura, K., Kataoka, Y. et al. (1997). Essential roles of the winged helix transcription factor MFH-1 in aortic arch patterning and skeletogenesis. *Development* **124**, 4627-4638.

Jawad, A. F., McDonald-Mcginn, D. M., Zackai, E. and Sullivan, K. E. (2001). Immunologic features of chromosome 22q11.2 deletion syndrome (DiGeorge syndrome/velocardiofacial syndrome). *J. Pediatr.* **139**, 715-723.

Jerome, L. A. and Papaioannou, V. E. (2001). DiGeorge syndrome phenotype in mice mutant for the T-box gene, Tbx1. *Nat. Genet.* **27**, 286-291.

Jiang, X., Rowitch, D. H., Soriano, P., McMahon, A. P. and Sucov, H. M. (2000). Fate of the mammalian cardiac neural crest. *Development* **127**, 1607-1616.

Kelly, R. G., Brown, N. A. and Buckingham, M. E. (2001). The arterial pole of the mouse heart forms from Fgf10-expressing cells in pharyngeal mesoderm. *Dev. Cell* **1**, 435-440.

Kimber, W. L., Hsieh, P., Hirotsune, S., Yuva-Paylor, L., Sutherland, H. F., Chen, A., Ruiz-Lozano, P., Hoogstraten-Miller, S. L., Chien, K. R., Paylor, R. et al. (1999). Deletion of 150 kb in the minimal DiGeorge/velocardiofacial syndrome critical region in mouse. *Hum. Mol. Genet.* **8**, 2229-2237.

Kirby, M. (1999). Contribution of neural crest to heart and vessel morphology. In *Heart Development* (ed. N. Rosenthal), pp. 179-193. San Diego, CA: Academic Press.

Kirby, M. L. and Waldo, K. L. (1990). Role of neural crest in congenital heart disease. *Circulation* **82**, 332-340.

Kurihara, Y., Kurihara, H., Oda, H., Maemura, K., Nagai, R., Ishikawa, T. and Yazaki, Y. (1995). Aortic arch malformations and ventricular septal defect in mice deficient in endothelin-1. *J. Clin. Invest.* **96**, 293-300.

Le Douarin, N. M. and Jotereau, F. V. (1975). Tracing of cells of the avian thymus through embryonic life in interspecific chimeras. *J. Exp. Med.* **142**, 17-40.

LeDouarin, N. (1982). *The Neural Crest*. Cambridge: Cambridge University Press.

LeLievre, C. S. and LeDouarin, N. (1975). Mesenchymal derivatives of the neural crest: analysis of chimaeric quail and chick embryos. *J. Embryol. Exp. Morphol.* **34**, 125-154.

Lewandoski, M., Sun, X. and Martin, G. R. (2000). Fgf8 signalling from the AER is essential for normal limb development. *Nat. Genet.* **26**, 460-463.

Lindsay, E. A. (2001). Chromosomal microdeletions: dissecting del22q11 syndrome. *Nat. Rev. Genet.* **2**, 858-868.

Lindsay, E. A. and Baldini, A. (2001). Recovery from arterial growth delay reduces penetrance of cardiovascular defects in mice deleted for the DiGeorge syndrome region. *Hum. Mol. Genet.* **10**, 997-1002.

Lindsay, E. A., Botta, A., Jurecic, V., Carattini-Rivera, S., Cheah, Y. C., Rosenblatt, H. M., Bradley, A. and Baldini, A. (1999). Congenital heart disease in mice deficient for the DiGeorge syndrome region. *Nature* **401**, 379-383.

Lindsay, E. A., Vitelli, F., Su, H., Morishima, M., Huynh, T., Pramparo, T., Jurecic, V., Ogunrinu, G., Sutherland, H. F., Scambler, P. J. et al. (2001). Tbx1 haploinsufficieny in the DiGeorge syndrome region causes aortic arch defects in mice. *Nature* **410**, 97-101.

MacArthur, C. A., Lawshe, A., Xu, J., Santos-Ocampo, S., Heikinheimo, M., Chellaiah, A. T. and Ornitz, D. M. (1995). FGF-8 isoforms activate receptor splice forms that are expressed in mesenchymal regions of mouse development. *Development* **121**, 3603-3613.

Manley, N. R. and Capecchi, M. R. (1998). Hox group 3 paralogs regulate the development and migration of the thymus, thyroid, and parathyroid glands. *Dev. Biol.* **195**, 1-15.

Mendelsohn, C., Lohnes, D., Decimo, D., Lufkin, T., LeMeur, M., Chambon, P. and Mark, M. (1994). Function of the retinoic acid receptors (RARs) during development (II). Multiple abnormalities at various stages of organogenesis in RAR double mutants. *Development* **120**, 2749-2771.

Merscher, S., Funke, B., Epstein, J. A., Heyer, J., Puech, A., Lu, M. M., Xavier, R. J., Demay, M. B., Russell, R. G., Factor, S. et al. (2001). TBX1 is responsible for cardiovascular defects in velo-cardio-facial/DiGeorge syndrome. *Cell* **104**, 619-629.

Meyers, E. N. and Martin, G. R. (1999). Differences in left-right axis pathways in mouse and chick: functions of FGF8 and SHH. *Science* **285**, 403-406.

Meyers, E. N., Lewandoski, M. and Martin, G. R. (1998). An Fgf8 mutant allelic series generated by Cre- and Flp-mediated recombination. *Nat. Genet.* **18**, 136-141.

Mitchell, P. J., Timmons, P. M., Hebert, J. M., Rigby, P. W. and Tjian, R. (1991). Transcription factor AP-2 is expressed in neural crest cell lineages during mouse embryogenesis. *Genes Dev.* **5**, 105-119.

Moon, A. M., Boulet, A. M. and Capecchi, M. R. (2000). Normal limb development in conditional mutants of Fgf4. *Development* **127**, 989-996.

Moon, A. M. and Capecchi, M. R. (2000). FGF8 is required for outgrowth and patterning of the limbs. *Nat. Genet.* **26**, 455-459.

Nakagawa, O., Nakagawa, M., Richardson, J. A., Olson, E. N. and Srivastava, D. (1999). HRT1, HRT2, and HRT3: a new subclass of bHLH transcription factors marking specific cardiac, somitic, and pharyngeal arch segments. *Dev. Biol.* **216**, 72-84.

Nakagawa, O., McFadden, D. G., Nakagawa, M., Yanagisawa, H., Hu, T., Srivastava, D. and Olson, E. N. (2000). Members of the HRT family of basic helix-loop-helix proteins act as transcriptional repressors downstream of Notch signaling. *Proc. Natl. Acad. Sci. USA* **97**, 13655-13660.

Orr-Urtreger, A., Bedford, M. T., Burakova, T., Arman, E., Zimmer, Y., Yayon, A., Givol, D. and Lonai, P. (1993). Developmental localization of the splicing alternatives of fibroblast growth factor receptor-2 (FGFR2). *Dev. Biol.* **158**, 475-486.

Orr-Urtreger, A., Givol, D., Yayon, A., Yarden, Y. and Lonai, P. (1991). Developmental expression of two murine fibroblast growth factor receptors, flg and bek. *Development* **113**, 1419-1434.

Peters, H., Neubuser, A., Kratochwil, K. and Balling, R. (1998). Pax9-deficient mice lack pharyngeal pouch derivatives and teeth and exhibit craniofacial and limb abnormalities. *Genes Dev.* **12**, 2735-2747.

Peters, K. G., Werner, S., Chen, G. and Williams, L. T. (1992). Two FGF receptor genes are differentially expressed in epithelial and mesemchymal tissues during limb formation and organogenesis in the mouse. *Development* **114**, 233-243.

Piotrowski, T. and Nusslein-Volhard, C. (2000). The endoderm plays an important role in patterning the segmented pharyngeal region in zebrafish (Danio rerio). *Dev. Biol.* **225**, 339-356.

Puech, A., Saint-Jore, B., Merscher, S., Russell, R. G., Cherif, D., Sirotkin, H., Xu, H., Factor, S., Kucherlapati, R. and Skoultchi, A. I. (2000). Normal cardiovascular development in mice deficient for 16 genes in 550 kb of the velocardiofacial/DiGeorge syndrome region. *Proc. Natl. Acad. Sci. USA* **97**, 10090-10095.

Revest, J. M., Suniara, R. K., Kerr, K., Owen, J. J. and Dickson, C. (2001). Development of the thymus requires signaling through the fibroblast growth factor receptor R2-IIIb. *J. Immunol.* **167**, 1954-1961.

Robinson, H. B., Jr (1975). DiGeorge's or the III-IV pharyngeal pouch syndrome: pathology and a theory of pathogenesis. *Perspect. Pediatr. Pathol.* **2**, 173-206.

Saint-Jore, B., Puech, A., Heyer, J., Lin, Q., Raine, C., Kucherlapati, R. and Skoultchi, A. I. (1998). Goosecoid-like (Gscl), a candidate gene for velocardiofacial syndrome, is not essential for normal mouse development. *Hum. Mol. Genet.* **7**, 1841-1849.

Scambler, P. J. (2000). The 22q11 deletion syndromes. *Hum. Mol. Genet.* **9**, 2421-2426.

Schorle, H., Meier, P., Buchert, M., Jaenisch, R. and Mitchell, P. J. (1996). Transcription factor AP-2 essential for cranial closure and craniofacial development. *Nature* **381**, 235-238.

Shprintzen, R. J., Goldberg, R. B., Lewin, M. L., Sidoti, E. J., Berkman, M. D., Argamaso, R. V. and Young, D. (1978). A new syndrome involving cleft palate, cardiac anomalies, typical facies, and learning disabilities: velo-cardio-facial syndrome. *Cleft Palate J.* **15**, 56-62.

Stadler, H. S., Higgins, K. M. and Capecchi, M. R. (2001). Loss of Eph-receptor expression correlates with loss of cell adhesion and chondrogenic capacity in Hoxa13 mutant limbs. *Development* **128**, 4177-4188.

Sun, X., Lewandoski, M., Meyers, E. N., Liu, Y. H., Maxson, R. E., Jr and Martin, G. R. (2000). Conditional inactivation of Fgf4 reveals complexity of signalling during limb bud development. *Nat. Genet.* **25**, 83-86.

Thomas, T., Kurihara, H., Yamagishi, H., Kurihara, Y., Yazaki, Y., Olson, E. N. and Srivastava, D. (1998). A signaling cascade involving endothelin-1, dHAND and msx1 regulates development of neural-crest-derived branchial arch mesenchyme. *Development* **125**, 3005-3014.

Trainor, P. and Krumlauf, R. (2000). Plasticity in mouse neural crest cells reveals a new patterning role for cranial mesoderm. *Nat. Cell Biol.* **2**, 96-102.

Trumpp, A., Depew, M. J., Rubenstein, J. L., Bishop, J. M. and Martin, G. R. (1999). Cre-mediated gene inactivation demonstrates that FGF8 is required for cell survival and patterning of the first branchial arch. *Genes Dev.* **13**, 3136-3148.

Tucker, A. S., Al Khamis, A., Ferguson, C. A., Bach, I., Rosenfeld, M. G. and Sharpe, P. T. (1999a). Conserved regulation of mesenchymal gene expression by Fgf-8 in face and limb development. *Development* **126**, 221-228.

Tucker, A. S., Yamada, G., Grigoriou, M., Pachnis, V. and Sharpe, P. T. (1999b). Fgf-8 determines rostral-caudal polarity in the first branchial arch. *Development* **126**, 51-61.

Van Mierop, L. H. and Kutsche, L. M. (1986). Cardiovascular anomalies in DiGeorge syndrome and importance of neural crest as a possible pathogenetic factor. *Am. J. Cardiol.* **58**, 133-137.

Veitch, E., Begbie, J., Schilling, T. F., Smith, M. M. and Graham, A. (1999). Pharyngeal arch patterning in the absence of neural crest. *Curr. Biol.* **9**, 1481-1484.

Wadey, R., McKie, J., Papapetrou, C., Sutherland, H., Lohman, F., Osinga, J., Frohn, I., Hofstra, R., Meijers, C., Amati, F. et al. (1999). Mutations of UFD1L are not responsible for the majority of cases of DiGeorge Syndrome/velocardiofacial syndrome without deletions within chromosome 22q11. *Am. J. Hum. Genet.* **65**, 247-249.

Wendling, O., Dennefeld, C., Chambon, P. and Mark, M. (2000). Retinoid signaling is essential for patterning the endoderm of the third and fourth pharyngeal arches. *Development* **127**, 1553-1562.

Yamagishi, H., Garg, V., Matsuoka, R., Thomas, T. and Srivastava, D. (1999). A molecular pathway revealing a genetic basis for human cardiac and craniofacial defects. *Science* **283**, 1158-1161.

Yanagisawa, H., Hammer, R. E., Richardson, J. A., Williams, S. C., Clouthier, D. E. and Yanagisawa, M. (1998). Role of Endothelin-1/Endothelin-A receptor-mediated signaling pathway in the aortic arch patterning in mice. *J. Clin. Invest.* **102**, 22-33.

Zhang, J., Hagopian-Donaldson, S., Serbedzija, G., Elsemore, J., Plehn-Dujowich, D., McMahon, A. P., Flavell, R. A. and Williams, T. (1996). Neural tube, skeletal and body wall defects in mice lacking transcription factor AP-2. *Nature* **381**, 238-241.